J. Appl. Comput. Mech., 4(3) (2018) 216-230
DOI: 10.22055/JACM.2017.23188.1150

ISSN: 2383-4536
jacm.scu.ac.ir

Shahid Chamran University of Ahvaz

Journal of Applied and Computational Mechanics

Research Article

The Complementary Functions Method (CFM) Solution to the Elastic Analysis of Polar Orthotropic Rotating Discs

Vebil Yıldırım

Department of Mechanical Engineering, Çukurova University, Adana, 01330, Turkey, email: vebil@cu.edu.tr

Received August 30 2017; Revised October 31 2017; Accepted for publication November 28 2017.
Corresponding author: Vebil Yıldırım, vebil@cu.edu.tr

Abstract. This study primarily deals with introducing an efficient numerical technique called the Complementary Functions Method (CFM) for the solutions of the initial value problem for the linear elastic analysis of anisotropic rotating uniform discs. To bring the performance of the method to light, first, closed form formulas are derived for such discs. The governing equation of the problem at stake is solved analytically with the help of the Euler-Cauchy technique under three types of boundary conditions namely free-free, fixed-free, and fixed-guided constraints. Secondly, the CFM is applied to the same problem. It was found that both numerical and analytical results coincide with each other up to a desired numerical accuracy. Third, after verifying the results with the literature, a parametric study with CFM on the elastic behavior of discs made up of five different materials which physically exist is performed. And finally, by using hypothetically chosen anisotropy degrees from 0.3 through 5, the effects of the anisotropy on the elastic response of such structures are investigated analytically. Useful graphs are provided for readers.

Keywords: Initial value problem (IVP); Exact elasticity solution; Polar orthotropic; Rotating disc.

1. Introduction

Rotating discs are essential structural components and continue to be used in a variety of engineering applications. For a very long time, researches have paid close attention to the stress and deformation analyses of stationary and rotating discs with uniform and variable thickness in mechanical engineering designs. These studies originated with the application of isotropic and homogeneous materials as a disc's principal material. In process of time, engineers became familiar with anisotropic materials [1-3] which enable engineers to increase the critical and burst speeds of such discs [4-29].

Tang [4] obtained closed-form stress solutions for rotating anisotropic discs with constant thickness for three cases: a solid disc, a disc mounted on a circular rigid shaft, and a disc with a circular hole at the center. Murthy and Sherbourne [5] presented analytical solutions for rotating stress-free anisotropic annular discs with variable thickness and a disc mounted on a circular rigid shaft (fixed-free). Reddy and Srinath [6] obtained closed-form solutions for stresses and displacement in an anisotropic rotating circular disc of variable thickness and variable density. They found that the stresses and displacement were lower when the mass density of material of the disc increased radially. They also presented graphically the degree of anisotropy and density variation on stresses and displacement. Chang [7] obtained closed-form stresses in a rotating disc or cylinder made of orthotropic material. He employed a semi-inverse technique for the material considered to be linear elastic and macroscopically homogeneous. Chang [8], in his another study, analytically obtained the stresses in rotating discs or cylinders made of general orthotropic material. The radial and circumferential stresses in a rotating circular disc were functions of radial coordinates only, and shear stress was equal to zero in Chang's [8] study. By using a laminated plate theory on layered plates with extension-bending coupling, Bert [9] obtained approximate solutions with stress-free boundaries. Gurushankar [10]

Published Online: June 13 2018

studied thermal stresses in a rotating nonhomogeneous anisotropic disc of varying thickness and density. Christensen and Wu [11] used anisotropic materials in the optimal design of flywheels. By defining the displacement field by means of both an algebraic and trigonometric series, Belingardi et al [12] approximately calculated the stress distribution in rotating discs made of orthotropic material. For uniform discs with and without a central hole, Belingardi et al. [12] concluded that the previous analytical solution for a disc with a central hole could give rise to unacceptable results. Genta and Gola [13] developed a particular closed-form solution for the constant thickness disc with a central hole made of an orthotropic material. Lekhnitskii [14] proposed a closed-form solution for the stress analysis in orthotropic disc and cylinders under pressure. Elishakoff [15] studied buckling of polar orthotropic circular plates resting on an elastic foundation in the context of Rayleigh's method. Oilin et al. [16] calculated the burst speed of aero engine disks. Employing the classical laminated plate theory, Tütüncü [17] determined the stresses and deformations resulting from centrifugal forces in rotating especially orthotropic circular plates. Tütüncü [17] also studied the effect of anisotropy with a stiffness ratio, which was defined as the ratio of circumferential stiffness to radial stiffness. The plate was assumed to be rigidly fixed to a concentric rod allowing no deformation in its central region. In Tütüncü's [17] study, the outer boundary was free of any constraints, or the plate was placed in a stiff casing which prevented radial deformation. Arnoldi et al. [18] addressed two major aspects of failure analysis, that is, the static and cyclic limit (burst) speeds for composite disks with constant thickness subjected to both internal pressure loading (as one would see in a hydro burst test) and pure rotation (as in the case of a free spinning disk). They graphically displayed their results (interaction diagrams) in a designer friendly format. Zhou and Ogawa [19] obtained elastic solutions of a rotating solid disc made of a cubic anisotropic material using direct displacement method. Displacement, strain, and stress distributions within the disc were expressed as simple functions of polar coordinates in the study. Çallıoğlu [20] conducted a stress analysis on a rotating hollow disc made of rectilinearly glass-fiber/epoxy prepreg under thermal loading. In another study, Çallıoğlu [21] carried out a thermal stress analysis of curvilinearly orthotropic rotating discs. Çallıoğlu et al. [22, 23] analytically investigated the elastic-plastic stress analysis of a curvilinearly orthotropic rotating annular disc for strain hardening material behavior. Sayer et al. [24] handled thermoelastic stress analysis in a thermoplastic curvilinearly fiber reinforced composite disk. Tahani et al. [25] analyzed deformation and stress fields in circumferentially fiber-reinforced composite rotating disks based on a semi-analytical method. Koo [26, 27] studied vibration analysis and critical speeds of polar orthotropic annular discs and composite laminated rotating discs. Alexandrova and Vila Real [28] offered a mathematical model for displacement and stress fields in elastic-perfectly plastic anisotropic annular disks. Nie et al. [29] investigated the material tailoring problem for a rotating disc composed of a radially inhomogeneous material to attain a constant hoop stress, a constant radial stress, or a constant in-plane shear stress throughout the disc. By the development of technology, and because of their impeccable heat-resistance features, orthotropic materials were supplanted by functionally graded materials (FGM). A functionally graded material may also be modelled as a non-homogeneous orthotropic material [30-38]. Zeng et al. [38] considered variable thickness discs, while others concentrated on uniform discs [30-37].

In this work, the elastostatic behavior of polar orthotropic rotating annular discs under three different boundary conditions is studied both analytically and numerically. The complementary functions method (CFM) is introduced for the numerical solution technique. The present analytical and numerical results are verified with the exact and numerical ones in the available literature. A comprehensive parametric study is conducted to consider the effects of polar orthotropic material types which physically exist, boundary conditions, and anisotropy degree on the radial variation of the radial displacement, radial stress, hoop stress, and von-Mises equivalent stress. Moreover, basic characteristics and each step of the CFM are more clearly explained in detail through the problem covered in the present study. In these respects, this study also offers a distinguished analysis in the related realm.

2. Governing Equation

By representing the derivatives of the related quantity with respect to the radial coordinate by the prime symbol, under the axisymmetric loading and plain-stress conditions, the strain- displacement relations in the infinitesimal theory of elasticity, $\varepsilon_{ij} - u_{ij}$, are written as:

$$\varepsilon_r(r) = u_r'(r), \quad \varepsilon_\theta(r) = \frac{u_r(r)}{r} \tag{1}$$

where u_r indicates the radial displacement, and ε_r and ε_θ stand for the radial and tangential strain components, respectively. The strain-displacement relations in Eq. (1) are used for both isotropic and polar orthotropic materials in the linear elastic analyses. By using the plain stress assumption for polar orthotropic materials, the stress-strain relations, that is, Hooke's law, take the following form:

$$\begin{Bmatrix}\sigma_r(r)\\ \sigma_\theta(r)\end{Bmatrix} = \begin{bmatrix}Q_{11} & Q_{12}\\ Q_{12} & Q_{22}\end{bmatrix}\begin{Bmatrix}\varepsilon_r(r)\\ \varepsilon_\theta(r)\end{Bmatrix} = \begin{bmatrix}\dfrac{E_r}{1-\nu_{r\theta}\nu_{\theta r}} & \dfrac{\nu_{r\theta}E_\theta}{1-\nu_{r\theta}\nu_{\theta r}}\\ \dfrac{\nu_{r\theta}E_\theta}{1-\nu_{r\theta}\nu_{\theta r}} & \dfrac{E_\theta}{1-\nu_{r\theta}\nu_{\theta r}}\end{bmatrix}\begin{Bmatrix}u_r'(r)\\ \dfrac{u_r(r)}{r}\end{Bmatrix} \tag{2}$$

where Q_{ij} terms are the transformed on-axis in-plane stiffness terms $(\theta = 0)$ or the elements of the transformed in-plane stiffness matrix of a lamina when a ply is rotated by an angle θ about the radial coordinate in case cross-ply symmetric laminates with respect to the radial coordinate or balanced symmetric laminates (see Appendix). The elements of the

transformed off-axis in-plane stiffness terms $(\theta \neq 0)$ are to be revisited in Section 5. In Eq. (2) Q_{11} and Q_{22} are referred to as the radial stiffness and the circumferential stiffness, respectively. In Eq. (2), σ_r and σ_θ also imply the radial and hoop stresses; $E_r(r)$ and $E_\theta(r)$ come to mean Young's modulus in the r and θ directions, respectively. Poisson's ratios, $v_{\theta r}$ and $v_{r\theta}$, are not independent but are related to each other as follows:

$$\frac{v_{\theta r}}{E_\theta} = \frac{v_{r\theta}}{E_r} \tag{3}$$

Equilibrium equation, in case a uniform disc or a circular annulus rotates at a constant angular velocity, ω, is (Fig. 1)

$$\sigma_r' + \left(\frac{\sigma_r - \sigma_\theta}{r}\right) + \rho\omega^2 r = 0 \tag{4}$$

where ρ denotes the material density. By substituting stresses in Eq. (2) and the first derivative of the radial stress with respect to the radial coordinate into the equilibrium equation given by Eq. (4) and replacing strain components with their counterpart radial displacement expressions given in Eq. (1), the following second order Navier differential equation with constant coefficients is derived in terms of the radial displacement:

$$u_r'' + \frac{u_r'}{r} - \frac{\lambda_2}{r^2}u_r = -\frac{\rho\omega^2}{Q_{11}}r \tag{5}$$

where the ratio of λ_2 denotes the anisotropy/polar degree of the disc material and indicates the ratio of circumferential stiffness to the radial stiffness. In the present study, an additional stiffness ratio, λ_1, is defined to make the parametric study easier and plausible as follows:

$$\begin{aligned} \lambda_1 &= \frac{Q_{12}}{Q_{11}} = \frac{E_\theta}{E_r} v_{r\theta} = \lambda_2 v_{r\theta} \\ \lambda_2 &= \frac{Q_{22}}{Q_{11}} = \frac{E_\theta}{E_r} = \frac{v_{\theta r}}{v_{r\theta}} \end{aligned} \tag{6}$$

2.1 Analytical Solution

By using Euler-Cauchy solution technique, the governing equation with constant coefficients in Eq. (5) is solved as follows:

$$u_r = r^{-\sqrt{\lambda_2}}\left(C_1 + r^{2\sqrt{\lambda_2}}C_2\right) - \frac{\rho\omega^2}{Q_{11}(9-\lambda_2)}r^3 = r^{-\xi/2}\left(C_1 + r^{\xi}C_2\right) + \Omega r^3 \tag{7}$$

where

$$\xi = 2\sqrt{\lambda_2}, \quad \Omega = \frac{\rho\omega^2}{Q_{11}(\lambda_2 - 9)} \tag{8}$$

In the absence of both the inner and outer pressures $(p_a = p_b = 0)$, the boundary conditions are to be used in the determination of integration constants in Eq. (7) to consider just centrifugal force effects. Let a, and b be the inner and outer radii of the disc, respectively (Fig. 1). As easily guessed, traction-free boundary conditions for rotating discs (Fig. 1c) are studied more extensively in the available literature, but the fixed-guided constraints have attracted less attention.

After determining the integration constants C_1 and C_2 according to the boundary conditions (Fig. 1), the radial displacement is obtained in the first place. Substitution of the first derivative and the radial displacement in Eq. (7) into Hooke's law in Eq. (2) gives both the exact radial and hoop stresses.

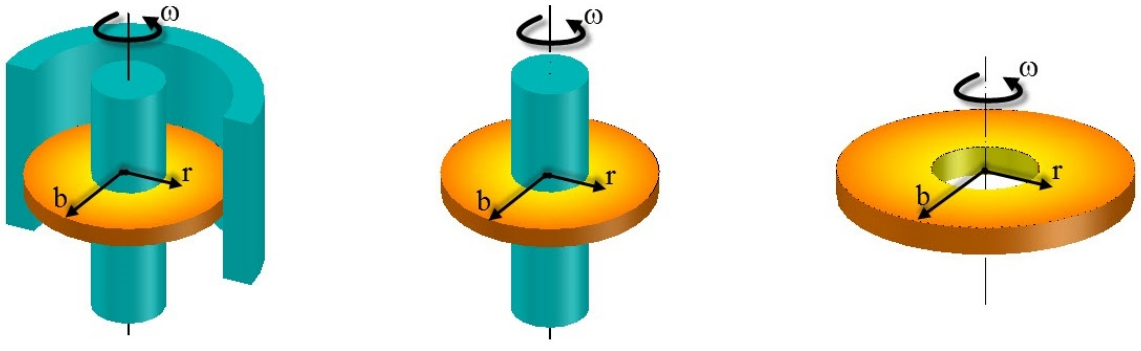

(a) (b) (c)

Fig. 1. a) A rotating disc with fixed-guided surfaces, b) A rotating disc mounted on a rotating rigid shaft, c) A rotating circular annulus

$$\sigma_r = Q_{11}\left(u_r' + \lambda_1 \frac{u_r}{r}\right) = \frac{1}{2} r^{\frac{1}{2}(-2-\xi)} \left[2Q_{12}\left(C_1 + C_2 r^{\xi}\right) + Q_{11}\left(C_2 r^{\xi}\xi - C_1\xi\right)\right] + r^2\Omega\left(Q_{12} + 3Q_{11}\right)$$
$$\sigma_\theta = Q_{11}\left(\lambda_1 u_r' + \lambda_2 \frac{u_r}{r}\right) = \frac{1}{2} r^{\frac{1}{2}(-2-\xi)} \left[2Q_{22}\left(C_1 + C_2 r^{\xi}\right) + Q_{12}\left(C_2 r^{\xi}\xi - C_1\xi\right)\right] + r^2\Omega\left(Q_{22} + 3Q_{12}\right) \tag{9}$$

Integration constants in Eq. (7) are found for free-free supported discs $\left(\sigma_r(a) = 0,\ \sigma_r(b) = 0\right)$ as (Fig. 1c),

$$C_1 = \frac{2\left(\lambda_1 + 3\right)\Omega a^{\xi} b^{\frac{1}{2}(\xi+6)} - 2\left(\lambda_1 + 3\right)\Omega b^{\xi} a^{\frac{1}{2}(\xi+6)}}{\left(a^{\xi} - b^{\xi}\right)\left(-2\lambda_1 + \xi\right)}$$
$$C_2 = \frac{2\left(\lambda_1 + 3\right)\Omega\left(a^{\frac{1}{2}(\beta+\xi+6)} - b^{\frac{1}{2}(\beta+\xi+6)}\right)}{\left(a^{\xi} - b^{\xi}\right)\left(\beta - 2\lambda_1 - \xi\right)} \tag{10}$$

for fixed-free supported discs $\left(u_r(a) = 0,\ \sigma_r(b) = 0\right)$ as (Fig. 1b),

$$C_1 = \frac{\Omega b^{\xi} a^{\frac{1}{2}(\xi+6)} 2\left(-2\lambda_1 - \xi\right) + 2\left(\lambda_1 + 3\right)\Omega a^{\xi} b^{\frac{1}{2}(\xi+6)}}{a^{\xi}\left(\beta - 2\lambda_1 + \xi\right) + b^{\xi}\left(-\beta + 2\lambda_1 + \xi\right)}$$
$$C_2 = -\frac{\Omega a^{\frac{1}{2}(\xi+6)}\left(-2\lambda_1 + \xi\right) + 2\left(\lambda_1 + 3\right)\Omega b^{\frac{1}{2}(\xi+6)}}{a^{\xi}\left(-2\lambda_1 + \xi\right) + b^{\xi}\left(2\lambda_1 + \xi\right)} \tag{11}$$

and finally for fixed-guided $\left(u_r(a) = 0,\ u_r(b) = 0\right)$ supported discs as follows (Fig. 1a):

$$C_1 = \frac{\Omega\left(b^{\xi} a^{\frac{1}{2}(\xi+6)} - a^{\xi} b^{\frac{1}{2}(\xi+6)}\right)}{a^{\xi} - b^{\xi}}$$
$$C_2 = \frac{\Omega\left(b^{\frac{1}{2}(\xi+6)} - a^{\frac{1}{2}(\xi+6)}\right)}{a^{\xi} - b^{\xi}} \tag{12}$$

It may be noted that solution (7) becomes unbounded when $\lambda_2 - 9 = 0$ for ordinary orthotropic materials.

2.2 Numerical Solution with CFM

The complementary functions method (CFM) is one of the methods profitably and truthfully used for the solution of initial value problems (IVP) [39-40]. Its central advantage over many methods is that it allows stable accurate numerical solution of ordinary differential equation sets even with variable coefficients up to any desired precision after converting the two-point boundary value problem (BVP) such as Eq. (5) into IVP such as the following.

$$\begin{Bmatrix} u_r'(r) \\ \sigma_r'(r) \end{Bmatrix} = \begin{bmatrix} -\dfrac{E_\theta \nu_{r\theta}}{r E_r} & -\dfrac{(\nu_{r\theta}\nu_{\theta r} - 1)}{E_r} \\ -\dfrac{E_\theta (E_r - E_\theta \nu_{r\theta}^2)}{E_r\, r^2 (\nu_{r\theta}\nu_{\theta r} - 1)} & \dfrac{E_\theta \nu_{r\theta}}{r E_r(r)} - \dfrac{1}{r} \end{bmatrix} \begin{Bmatrix} u_r(r) \\ \sigma_r(r) \end{Bmatrix} + \begin{Bmatrix} 0 \\ -\rho(r)\omega^2 r \end{Bmatrix} \tag{13}$$

Under axisymmetric loading and plane-stress conditions, Eqs. (5) and (13) govern the elastostatic behavior of uniform discs made of polar orthotropic materials, which rotate at a constant angular velocity, ω, about the axis passing through its center. As one may easily guess, for isotropic and homogeneous materials: $E = E_\theta = E_r$.

The authors have also employed this method directly or used it as an assistive method in some static, buckling, and dynamic problems [41-46]. In the present study, CFM is to be first directly applied to the elastic behavior of rotating polar orthotropic uniform discs. In the IVP, it is necessary to transform a second order differential equation into two first-order differential equation sets. The principal variables in the IVP may be chosen in different ways. For example, in general, the IVP transformation with variables $z_1 = u_r$ and $z_2 = u_r'$ is frequently adopted instead of using variables $z_1 = u_r$ and $z_2 = \sigma_r$, which is the most convenient form of the problem available, as in the present study.

To explain CFM, the frequently chosen variables, $z_1 = u_r$ and $z_2 = u_r'$ are used as the principal variables of the IVP. This labelling also means that $z_1' = u_r' = z_2$ and $z_2' = u_r''$. To transform BVP into IVP, the governing equation, Eq. (5), is rewritten in terms of only z_1, z_2, and their first derivatives.

$$z_2' + \frac{1}{r} z_2 - \frac{\lambda_2}{r^2} z_1 = -\frac{\rho\omega^2}{Q_{11}} r \tag{14}$$

Then, the following, which describes the IVP form of Eq. (5), may be easily obtained:

$$\begin{Bmatrix} z_1'(x) \\ z_2'(x) \end{Bmatrix} = \begin{bmatrix} 0 & 1 \\ \dfrac{\lambda_2}{r^2} & -\dfrac{1}{r} \end{bmatrix} \begin{Bmatrix} z_1(x) \\ z_2(x) \end{Bmatrix} + \begin{Bmatrix} 0 \\ -\dfrac{\rho\omega^2}{Q_{11}} \end{Bmatrix} \tag{15}$$

where the last term at the right side is called the nonhomogeneous term. Under the chosen physical boundary conditions, in CFM, the general solution of Eq. (5) over the interval [*a*, *b*] is given by [39-40]:

$$u_r(x) = u_0(x) + b_1 u_1(x) + b_2 u_2(x) \tag{16}$$

where $u_0(x)$ is the particular solution of Eq.(15), while $u_1(x)$ and $u_2(x)$ are the homogeneous solutions of the same equation, which should be linearly independent. As expected, b_1 and b_2 are constants which should be determined from the given physical boundary conditions of the chosen problem. In all the four solution stages in CFM, all terms at the right side $u_0(x), u_1(x), u_2(x)$, b_1 and b_2 are to be determined.

The prescribed boundary conditions consisting of either initial zero conditions or initial Kronecker delta conditions are first used to find $u_0(x), u_1(x)$ and $u_2(x)$ with the help of either the particular or the homogeneous solution of Eq. (15) in the first three stages. In the final stage, the given physical boundary conditions such as $u_r(a) = 0$ and $u_r(b) = 0$ are considered to determine unknown constants b_1 and b_2 by using the solution given in Eq. (16). Then, the numerical solution procedure becomes complete.

In the first stage let $z_1 = u_0, z_2 = u_0'$, solve Eq. (15) with non-homogeneous term under the first prescribed boundary conditions that is under zero initial conditions, $z_1(a) = 0, z_2(a) = 0$ and get the particular solution, $u_0(x)$, and its derivative $u_0'(x)$, at the same time. In the second stage, let $z_1 = u_1, z_2 = u_1'$. Solution of Eq. (15) without non-homogeneous term under the second prescribed boundary conditions $z_1(a) = 1, z_2(a) = 0$ gives the first homogeneous solution $u_1(x)$ and its derivative $u_1'(x)$, simultaneously. In the third stage, after letting $z_1 = u_2, z_2 = u_2'$, again solve Eq. (15) without non-homogeneous term under prescribed boundary conditions $z_1(a) = 0, z_2(a) = 1$ to reach the last homogeneous solution $u_2(x)$ and its derivative $u_2'(x)$, at once. After imposing $u_0(x), u_1(x)$ and $u_2(x)$ into the general solution, Eq. (16), the physical boundary conditions of the differential equations such as Eq. (17) should now be applied to determine the remaining unknown coefficients b_1 and b_2 in a straight forward manner. For example, for fixed-guided discs (Fig. 1) the following may be written.

$$\begin{aligned} u_r(a) &= u_0(a) + b_1 u_1(a) + b_2 u_2(a) = 0 \\ u_r(b) &= u_0(b) + b_1 u_1(b) + b_2 u_2(b) = 0 \end{aligned} \tag{17}$$

This gives:

$$\begin{bmatrix} u_1(a) & u_2(a) \\ u_1(b) & u_2(b) \end{bmatrix} \begin{Bmatrix} b_1 \\ b_2 \end{Bmatrix} = \begin{Bmatrix} -u_o(a) \\ -u_o(b) \end{Bmatrix} \tag{18}$$

This is a linear equation set of order two; therefore, the solution may be written readily in an explicit form as follows:

$$\begin{aligned} b_1 &= \frac{\begin{vmatrix} -u_o(a) & u_2(a) \\ -u_o(b) & u_2(b) \end{vmatrix}}{\begin{vmatrix} u_1(a) & u_2(a) \\ u_1(b) & u_2(b) \end{vmatrix}} = \frac{-u_o(a)u_2(b) + u_o(b)u_2(a)}{u_1(a)u_2(b) - u_1(b)u_2(a)} \\ b_2 &= \frac{\begin{vmatrix} u_1(a) & -u_o(a) \\ u_1(b) & -u_o(b) \end{vmatrix}}{\begin{vmatrix} u_1(a) & u_2(a) \\ u_1(b) & u_2(b) \end{vmatrix}} = \frac{-u_o(b)u_1(a) + u_o(a)u_1(b)}{u_1(a)u_2(b) - u_1(b)u_2(a)} \end{aligned} \tag{19}$$

The solution process comes to an end by substitution of b_1 and b_2 in the general solution of the radial displacement, Eq. (16). As understood from the above, $z_1 = u_r(r)$ and $z_2 = u_r'(r)$ are concurrently obtained at the end of the four stages of CFM. This may be helpful for much more advanced studies. After determining the radial displacement and its derivatives as explained above, the radial stress and the tangential stress (hoop stress) are achieved from Hooke's law in Eq. (2). As a final remark, it may be noted that, in the first three stages, which require the numerical solution of the first degree ordinary

differential equations which may be either nonhomogeneous or homogeneous form, a procedure like RK4 or RK5 from Runge-Kutta family may be used.

3. Verification of the Results

As a comparative example, a disc with *a=2cm* and *b=5cm* is chosen [35]. The disc is made of an injection molded Nylon 6 composite containing 40wt% short glass fiber (MAT-5). The material properties are given in Table 1. The dimensionless elastic stress and displacements are defined as:

$$\bar{\sigma}_r = \frac{\sigma_r}{\rho_b \omega^2 b^2}, \quad \bar{\sigma}_\theta = \frac{\sigma_\theta}{\rho_b \omega^2 b^2}, \quad \bar{u}_r = \frac{E_\theta}{\rho_b \omega^2 b^3} u_r \tag{20}$$

Comparisons of dimensionless radial displacements, radial stresses, and hoop stresses with the literature for MAT-5 are presented in Table 2 for traction-free discs. Table 2 depicts a perfect synchronization of the results. Table 2 also verifies that RK4 is basic but a sufficiently powerful technique in the numerical solution procedure to be used in the solution of these types of problems.

Table 1. Anisotropic materials and their properties

	Label	E_r (GPa)	E_θ(GPa)	ρ ($\frac{\text{kg}}{m^3}$)	$\nu_{r\theta}$
Polycarbonate [26]	MAT-1	2.2	2.2	1220	0.3
GFRP (E-Glass/Epoxy) [26]	MAT-2	28.6	8.27	1800	0.26
CFRP (T300/N5208) [26]	MAT-3	181.	10.3	1600	0.28
A Glass Fiber/Epoxy Prepreg [21-23]	MAT-4	21.8	26.95	2030	0.15
An injection molded Nylon 6 composite containing 40wt% short glass fiber [21-23, 35]	MAT-5	12.0	20.0	1600	0.21

Table 2. Comparison of dimensionless radial displacement, radial stress, and hoop stress with the literature for MAT-5 under stress-free boundary condition

a/b	Exact (Present)	Exact [35]	Numerical [35]	Numerical (Present)	Numerical [36]
			$\bar{u}_r$		
0.4	0.329539158	0.3295	0.3295	0.3295391	0.3295391
0.5	0.314078601	0.3141	0.3142	0.3140786	0.3140785
0.6	0.313829940	0.3138	0.3141	0.3138299	0.3138298
0.7	0.318607411	0.3186	0.3189	0.3186074	0.3186073
0.8	0.322816974	0.3228	0.3229	0.3228170	0.3228169
0.9	0.322827116	0.3228	0.3229	0.3228271	0.3228270
1	0.315959666	0.3160	0.3160	0.3159597	0.3159597
			$\bar{\sigma}_r$		
0.4	0	0	0	0	0
0.5	0.106551013	0.1066	0.1067	0.1065510	0.1065510
0.6	0.140870514	0.1409	0.1409	0.1408705	0.1408704
0.7	0.136928401	0.1369	0.1367	0.1369284	0.1369283
0.8	0.108397223	0.1084	0.1086	0.1083972	0.1083971
0.9	0.061651073	0.0617	0.0618	0.06165107	0.06165102
1	0	0		0	0
			$\bar{\sigma}_\theta$		
0.4	0.823847895	0.8238	0.8238	0.8238477	0.8238477
0.5	0.665450057	0.6655	0.6654	0.6654500	0.6654499
0.6	0.572354580	0.5724	0.5722	0.5723545	0.5723544
0.7	0.503078385	0.5031	0.5027	0.5030784	0.5030782
0.8	0.441460245	0.4415	0.4420	0.4414602	0.4414601
0.9	0.380274671	0.3803	0.3805	0.3802747	0.3802746
1	0.315959666	0.3160	0.3160	0.3159597	0.3159597

4. Examples with CFM

In this section, some problems related to uniform rotating discs made of physical anisotropic materials whose properties are given in Table 1 are to be considered. The anisotropy degrees of the physical materials are presented in Table 3. The same inner and outer radii, *a=2cm* and *b=5cm*, are to be used for the disc geometry as in the previous section. The equivalent stress based on von-Mises failure criteria under plane-stress assumption is defined as:

$$\sigma_{eq} = \sqrt{\sigma_r^2 - \sigma_r \sigma_\theta + \sigma_\theta^2} \tag{21}$$

Numerical values of the dimensionless tangential stresses at the inner surface for different types of physical materials and

boundary conditions are exhibited in Table 4. This table shows that the tangential stresses at the inner surface are higher than the outer surface under free-free conditions. The minimum circumferential stresses are obtained at the inner surface for the disk having fixed-guided surfaces.

Table 3. λ_1 and λ_2 ratios of physical materials presented in Table 2

	$\lambda_1 = \nu_{r\theta}$	$\lambda_2 = E_\theta/E_r$
MAT-1	0.3	1
MAT-2	0.075	0.289
MAT-3	0.016	0.057
MAT-4	0.185	1.236
MAT-5	0.35	1.667

Table 4. Dimensionless tangential stresses at the inner surface for different materials and boundary conditions

	$\bar{\sigma}_\theta(a)$		
	Free-Free	Fixed-Free	Fixed-Guided
MAT-1	0.8529999	0.1522351	0.06300001
MAT-2	0.8492961	0.05094031	0.01685186
MAT-3	0.8511305	0.01205892	0.003651363
MAT-4	0.8151127	0.09269719	0.03813651
MAT-5	0.8238477	0.1510878	0.06935726

4.1 Stress-Free Boundaries

Variations of the dimensionless radial displacement, radial, hoop, and von-Mises equivalent stresses along the radial direction with free-free boundary condition and physical anisotropic materials are illustrated in Fig. 2. The following are observed in Fig. 2:

* The materials MAT-1, MAT-4, and MAT-5, which have $\lambda_2 \geq 1$, show all symmetric wave-like radial displacement variations along the radial direction. This was also observed in Peng and Li's study [35]. When $\lambda_2 < 1$, this wave-like variation becomes too small to be noticed as in MAT-2 and MAT-3.

Fig. 2. Variation of the elastic quantities with material types for free-free boundary conditions

* MAT-3 offers maximum radial displacements.
* Maximum radial displacements are mostly at the inner surface for all materials except for MAT-4.
* Radial stresses at both surfaces vanish. This situation is consistent with the surface free boundary conditions. In the

intermediate surfaces, radial stresses are all in tension. Maximum radial stress occurs around the middle surface slightly closer to the inner surface for all types of materials. Although they are very close to each other, the radial stresses are higher to some extent for orthotropic materials with $\lambda_2 \leq 1$ than the others.

* Maximum radial stress is around one sixth of the maximum tangential stress.

* The tangential stresses and equivalent stresses which are all in tension show familiar radial variation. They increase monolithically by increasing the radial coordinate. The maximum hoop stress and equivalent stress are at the inner surface.

* The curves of equivalent stresses are almost in the same character of the curves of hoop stresses, since circumferential stresses are dominant for free-free boundaries.

* Maximum hoop and equivalent stresses are observed in materials MAT-2 and MAT-3, whose orthotropic degrees are less than unit, $\lambda_2 < 1$.

4.2 Fixed-Free Boundaries

Variations of the dimensionless radial displacement, radial, hoop, and von-Mises equivalent stresses along the radial direction with fixed-free boundary condition and the materials in Table 1 are illustrated in Fig. 3. The following conclusions may be drawn from Fig. 3:

* Radial displacements diminish at the inner surface, while the radial stresses vanish at the outer surface in accordance with the applied boundary conditions.

* The radial displacements progressively increase from the inner surface towards the outer surface.

* Both the radial stresses and equivalent stresses decrease by increasing radial coordinate.

* For this boundary condition, the influence of the radial stresses over the hoop stresses seems to be increased.

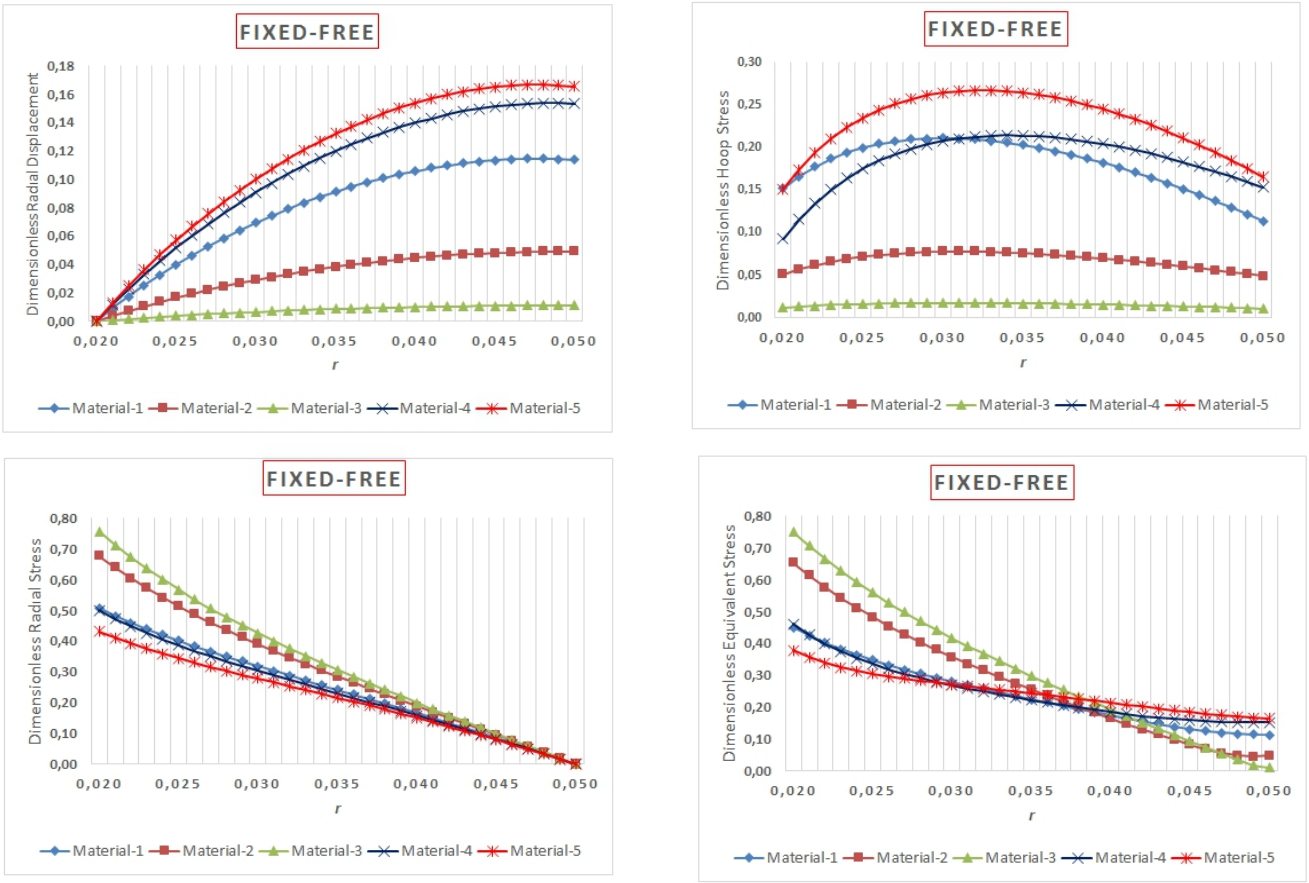

Fig. 3. Variation of the elastic quantities with material types for fixed-free boundary conditions

* The anisotropic materials having greater anisotropy degree exhibit much higher radial displacements. In other words, MAT-5 has the highest radial displacement, followed by MAT-4, MAT-1, MAT-2, and MAT-3, respectively.

* Variations of the hoop stresses along the radial direction may be different with respect to the type of materials. For example, the maximum hoop stress is around the middle surface for both MAT-5 and MAT-4. Among them, MAT-5 has the maximum hoop stress. The maximum hoop stress in MAT-1 is observed at the region very close to the inner surface. For MAT-2 and MAT-3, the differences in the magnitudes of the hoop stresses at both surfaces are very small.

* MAT-5 shows almost symmetric behavior in the variation of the hoop stresses.

* The maximum radial stresses occur at the inner surface. MAT-3 having the smallest λ_1 and λ_2 ratios in all materials in Table 2, offers the highest maximum radial stress, followed by MAT-2, MAT-4, and MAT-1, respectively. MAT-5 has the smallest maximum radial stress.

* It may be observed that when the anisotropy degree increases, the numerical value of the maximum radial stress

decreases.

* The variations of both the radial stress and equivalent stress curves show similar characteristics with the same order of materi al types.

4.3 Fixed-Fixed Boundaries

Variations of the dimensionless radial displacement, radial, hoop, and von-Mises equivalent stresses along the radial coordinate with fixed-fixed boundary condition and the materials in Table 1 are illustrated in Fig. 4. The outcomes that can be extracted from Fig. 4 may be as follows:

* The radial stresses vanish at both the inner and outer surfaces as compared with the boundary conditions.

* The maximum radial displacements occur at the vicinity of the middle surface. MAT-5 followed by MAT-4, MAT-1, MAT-2, and MAT-3, respectively, gives the highest radial displacement.

* MAT-3 presents almost no radial displacement.

* The absolute values of the maximum radial stress are almost twice of the maximum hoop stresses.

* MAT-2 followed by MAT-3 has the highest radial stresses.

* Radial stresses may have almost symmetric variation with respect to the middle surface. They may be in both tension and compression. Tensions are located at the inner surface of the disc.

* The tension-compression behavior is also observed in the variation of hoop stresses. However, this is not full symmetric. The maximum hoop stresses are either at the inner surface or at the vicinity of the inner surface of the disc. Compressions occur at the outer surface.

* The highest hoop stresses are observed in MAT-5 followed by MAT-1, MAT-4, MAT-2, and MAT-3, respectively.

* MAT-3 has almost stable variation for the hoop stresses.

* The variation of the equivalent stresses takes almost a symmetric form due to the existence of compressions at the outer surface for both the radial and hoop stresses.

* MAT-3 followed by MAT-2, MAT-1, MAT-4, and MAT-5, respectively, gives the smallest equivalent stresses at the middle surface of the disc. MAT-3 followed by MAT-2, MAT-2, MAT-1, MAT-4, and MAT-5, respectively, also shows the highest equivalent stresses.

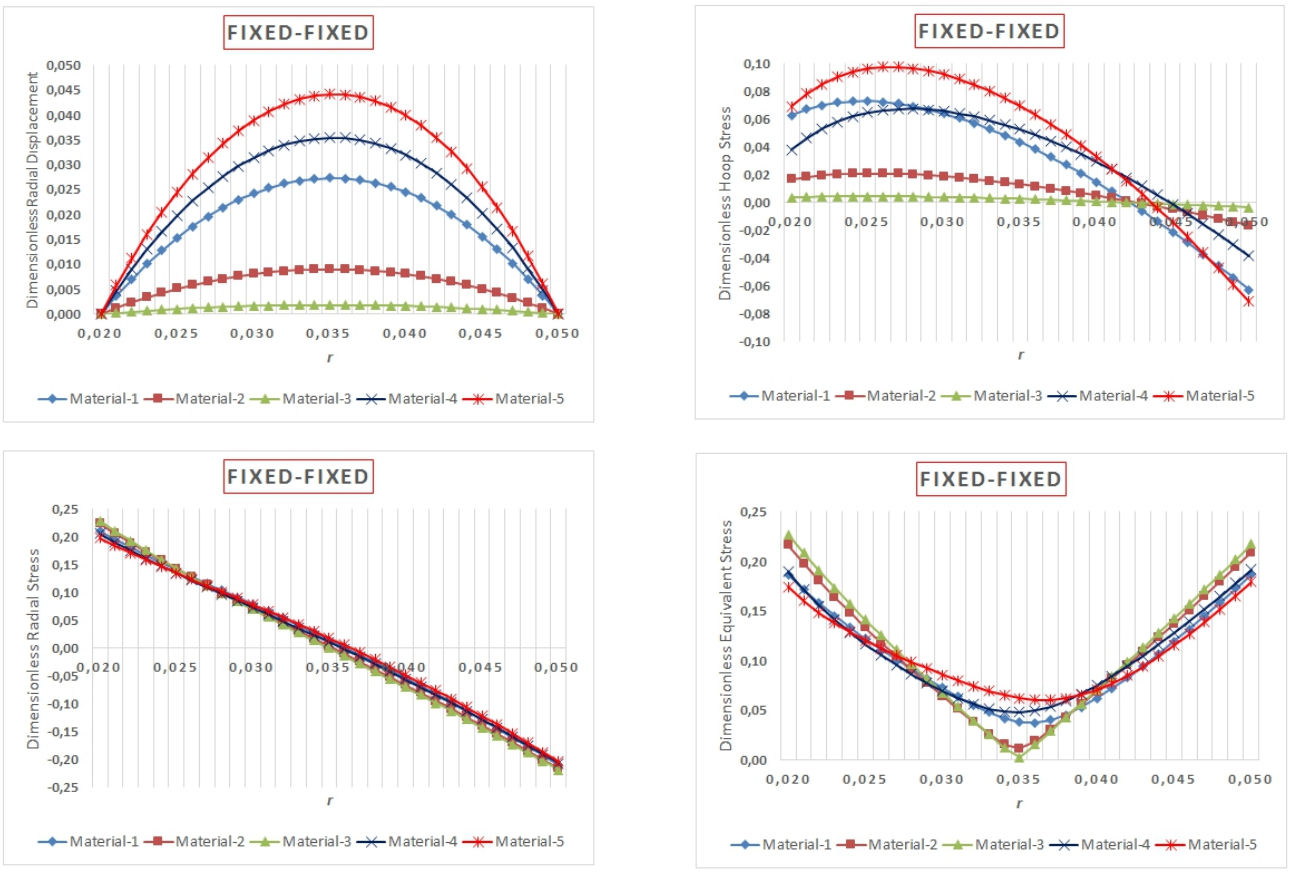

Fig. 4. Variation of the elastic quantities with material types for fixed-fixed boundary conditions

5. Investigation of Anisotropy Effects

To study the effect of the fiber orientation angle θ, reconsider Q_{ij} which is an element of the transformed in-plane stiffness matrix of a lamina when a ply is rotated by an angle θ about the radial axis. By referring to directions along the fiber

and transverse to the fiber by subscripts x and y, respectively, and denoting the in-plane shear by subscript s, the transformed off-axis in-plane stiffness terms are given in Appendix ($\theta \neq 0$). As expected, different transformed stiffness terms and eventually different resultant stresses through the thickness of a laminate may be developed according to the chosen anisotropic material types and/or fiber orientations of each lamina for the same material. Stress discontinuities at ply interfaces may also occur at some fiber orientations in each ply. As stated above, λ_2 is referred to as the anisotropy degree of the inhomogeneous material and indicates the ratio of circumferential stiffness to the radial stiffness. As a numerical example, consider an anisotropic material (CFRP (T300/N5208) of $E_x = 181.0\ GPa$; $E_y = 10.3\ GPa$; $E_s = 7.17\ GPa$; $\nu_{xy} = 0.28$, and labelled by MAT-3) in Table 1.

Table 5. Corresponding fiber angles for a certain anisotropy degree ($0° \leq \theta \leq 90°$)

λ_2	0.3	0.4	0.5	0.6	0.7	0.8	0.9	1	2
$\pm\theta$ (°)	33.39	36.24	38.40	40.15	41.62	42.89	44.00	45	51.60
λ_2	3	4	5	6	7	8	9	10	17.19
$\pm\theta$ (°)	55.56	58.47	60.84	62.87	64.69	66.37	67.97	69.53	85.27

Corresponding fiber angles for a certain anisotropy degree for the chosen material are given in Table 5 for ($0° \leq \theta \leq 90°$). The angles may be originated from either the cross-ply symmetrical laminates (namely all the plies are oriented at 0 ° and 90 ° with respect to the radial coordinate axis) or the balanced symmetrical laminates (plies oriented at $\pm\theta$, that is, for each ply oriented $+\theta$ there must exists a ply oriented at $-\theta$). As stated above, the same anisotropy degrees for specially orthotropic laminates may also be obtained by placing stiffeners in the very radial and circumferential directions. Variation of the ratios of the transformed stiffness terms with respect to the fiber orientation angle ($0° \leq \theta \leq 90°$) is presented in Figure 5.

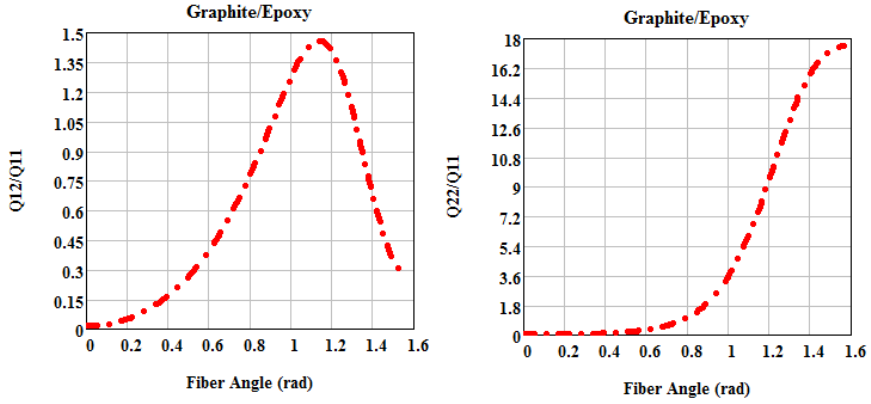

Fig. 5. Variation of the ratios of the transformed stiffness terms with respect to the fiber orientation angle

As shown in Fig. 5 and Table 6, $\lambda_2 = 9$ corresponds to the fiber orientation angle of θ =$\pm$67.974°, in other words, $(\pm 67.974°)_s$ laminate configurations. As stated above, for ordinary orthotropic materials, solution (7) becomes unbounded at $\lambda_2 = 9$. It is also clearly seen in Fig. 5 that the anisotropy degree curve has an inflection point when $\lambda_2 = 9$. The overweight of circumferential stiffness on the radial stiffness increases at a snail's pace from $\lambda_2 = 0$ through $\lambda_2 = 1$. However, when $\lambda_2 > 1$ the supremacy of the circumferential stiffness on the radial stiffness increases by leaps and bounds. In the present study, for some values of the anisotropy ratios between 0.3 and 5 ($0.3 \leq \lambda_2 \leq 5$), variations of the radial displacements, the radial stress, and the hoop stress with the anisotropy degrees and boundary conditions are graphically illustrated in Figs. 6, 7 and 8. As stated above, the anisotropy degrees are chosen hypothetically in this section. However, the values of the other ratio, λ_1, are chosen as $\lambda_1 = 0.28\lambda_2$ in accordance with the polar orthotropic character.

Consider Fig. 6.

* For fixed-guided ends, the maximum radial displacement is placed almost at the mid-way surface when $\lambda_2 < 1$. The maximum radial displacement begins to shift towards the outer surface by increasing anisotropy degrees greater than 1. Radial displacement increases by increasing anisotropy degree from 0.3 to 5.

* For fixed-free ends, the radial displacements steadily buildup by increasing anisotropy degrees towards the outer surface of the disc.

* For free-free ends, while the maximum radial displacement comes about at the inner surface of the disk for $0.3 < \lambda_2 < 0.6$, it occurs at the outer surface at higher degrees of $\lambda_2 > 0.6$ in accordance with the wave-like variation with the radial coordinate.

Fig. 7 shows that:

* For fixed-guided ends, the radial stress may be either in tension or compression in nature. For both $0.3 \leq \lambda_2 \leq 0.9$ and $1 \leq \lambda_2 \leq 5$, the radial stress decreases by increasing anisotropy degrees. The differences in the decrease are more notable for the anisotropy degree greater than unit. While the tension stresses are placed at the inner surface, the compression stresses are located at the outer surface.

* For fixed-free ends, radial stresses decrease by increasing anisotropy degree. The maximum radial stress occurs at the inner surface. It may be concluded from the figure that, for anisotropy degrees greater than 5, the radial stress at the inner surface starts to be diminished, whereas the maximum radial stress begins to emerge at the vicinity of the inner surface. This means that when circumferential stiffness is more than five times higher than radial stiffness, the hoop fibers carry more load

than the radial fibers; eventually, the radial stress at the inner surface is weakened.

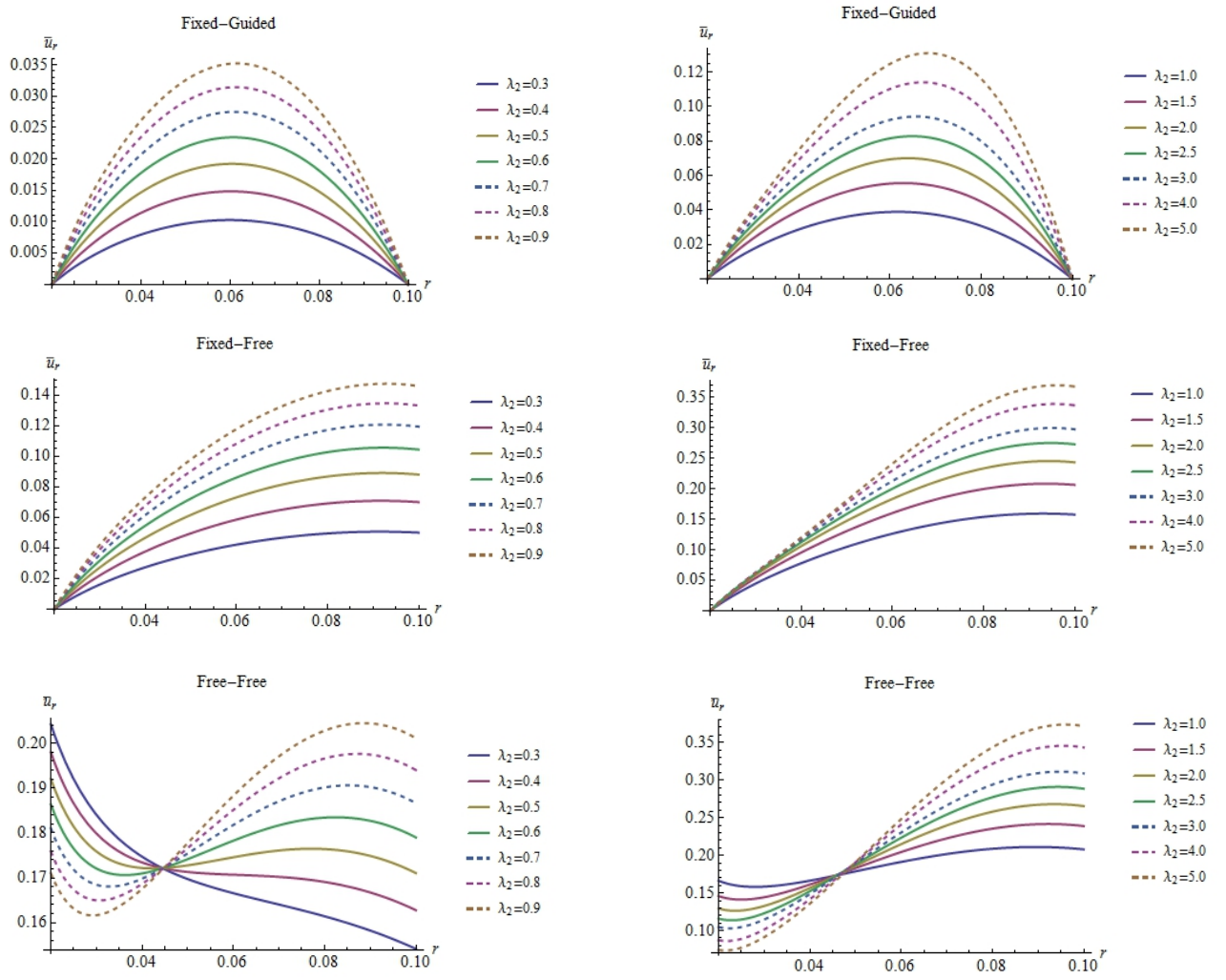

Fig. 6. Variation of the radial displacements with the anisotropy degrees and boundary conditions (*a=2cm, b=10 cm*) ($0.3 \leq \lambda_2 \leq 5$)

* For free-free ends, increasing anisotropy degrees makes maximum radial stresses which are close to the inner surface much smaller.

The following conclusions may be achieved from Fig. 8:

* For fixed-guided surfaces, as the anisotropy degree increases, the maximum hoop stresses increase. While tensions are at the inner surface, compressions are at the outer surface. Maximum hoop stresses are in the vicinity of the inner surface. As the anisotropy degree increases, the location of the maximum hoop stress shifts to the middle surface.

* In both fixed-free and free-free boundary conditions, hoop stresses are all in tension.

* As the anisotropy degree increases, the magnitudes of hoop stresses increase under all boundary conditions.

* Maximum hoop stresses are observed at the inner surface for free-free, at either inner or outer surface for fixed-free, and at either the vicinity of the inner or mid-way surfaces for fixed-fixed discs.

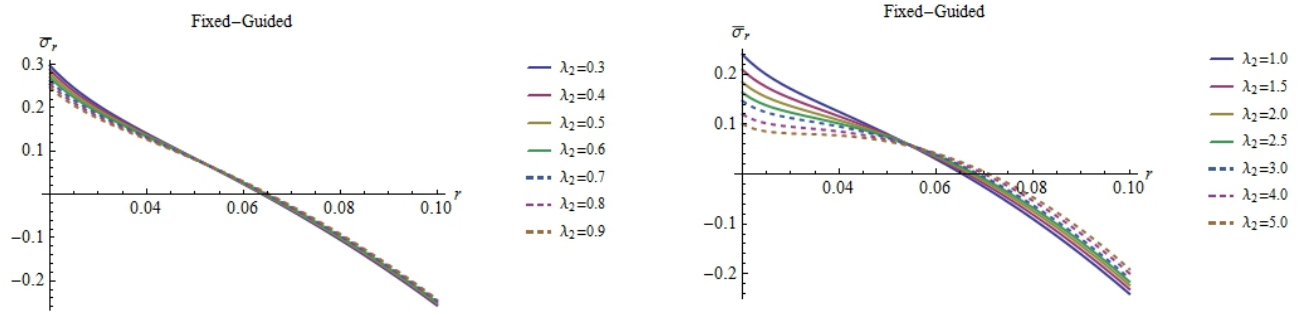

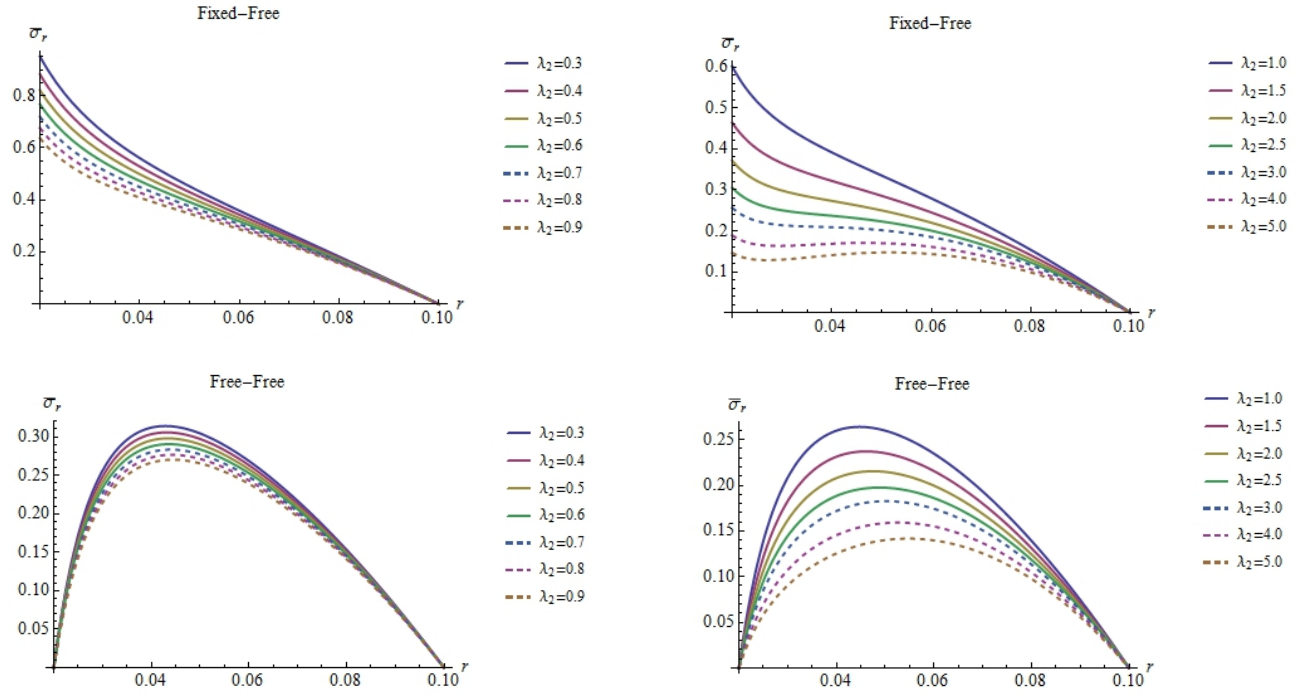

Fig. 7. Variation of the radial stresses with the anisotropy degrees and boundary conditions (*a=2cm, b=10 cm*) ($0.3 \leq \lambda_2 \leq 5$)

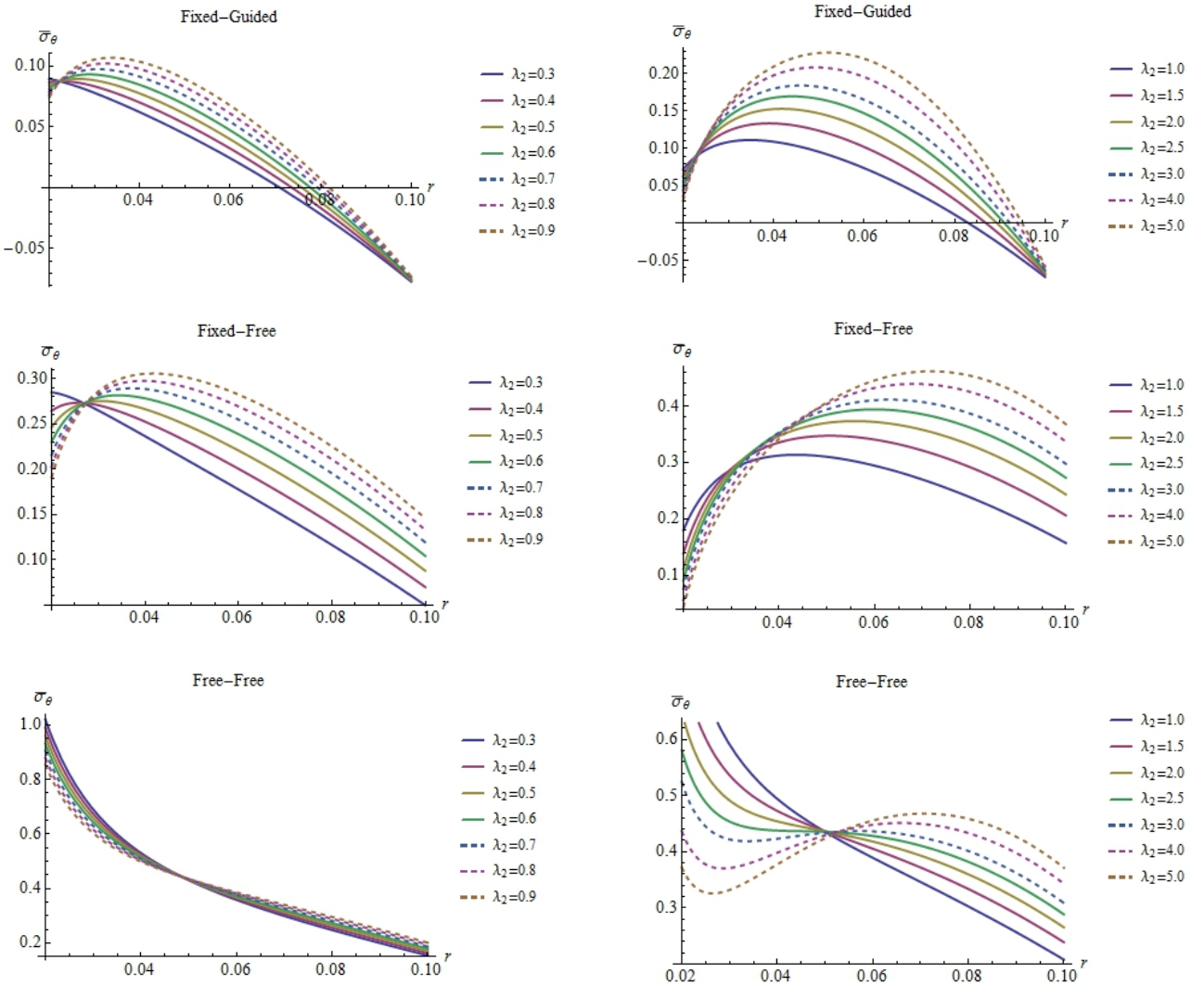

Fig. 8. Variation of the hoop stresses with the anisotropy degrees and boundary conditions (*a=2cm, b=10 cm*) ($0.3 \leq \lambda_2 \leq 5$)

6. Conclusion

The fact that rotating discs made of a polar orthotropic material have not been studied comprehensively was the motivation of the present study. In this work, compact analytical formulas are offered for determination of the elastic response of rotating polar orthotropic uniform discs under three different boundary conditions. The same problem is also originally solved numerically by an efficient initial value problem solution technique called the complementary functions method (CFM). The perfect accordance is observed between the analytical and numerical solutions. After validation of the results, parametric studies by both analytical formulas and numerical CFM results are conducted to study the elastic behavior of such discs made of either physically anisotropic or hypothetically anisotropic materials. Quite useful results about the general elastic behavior of such discs are obtained, which are exhibited by graphs for the readers. The present study also reveals that CFM is a powerful and an accurate numerical method to be applied to advanced studies of such structures.

Appendix

The transformed off-axis in-plane stiffness terms are $(\theta \neq 0)$

$$\begin{aligned} Q_{11} &= c^4 Q_{xx} + s^4 Q_{yy} + 2c^2 s^2 Q_{xy} + 4c^2 s^2 Q_{ss} \\ Q_{12} &= c^2 s^2 Q_{xx} + c^2 s^2 Q_{yy} + (c^4 + s^4) Q_{xy} - 4c^2 s^2 Q_{ss} \\ Q_{11} &= s^4 Q_{xx} + c^4 Q_{yy} + 2c^2 s^2 Q_{xy} + 4c^2 s^2 Q_{ss} \end{aligned} \tag{A1}$$

where

$$c = \cos\theta,\ s = \sin\theta, v_{yx} = \frac{E_y}{E_x} v_{xy} \tag{A2}$$

The transformed on-axis in-plane stiffness terms are $(\theta = 0)$

$$\begin{aligned} Q_{xx} &= \frac{1}{1 - v_{xy}^2 \dfrac{E_y}{E_x}} E_x = -\frac{E_y v_{xy}}{v_{yx}\left(v_{xy} v_{yx} - 1\right)} \\ Q_{xy} &= \frac{1}{1 - v_{xy}^2 \dfrac{E_y}{E_x}} E_x v_{yx} = -\frac{E_y v_{xy}}{\left(v_{xy} v_{yx} - 1\right)} \\ Q_{yy} &= \frac{1}{1 - v_{xy}^2 \dfrac{E_y}{E_x}} E_y = -\frac{E_y}{\left(v_{xy} v_{yx} - 1\right)} \\ Q_{ss} &= E_s \end{aligned} \tag{A3}$$

References

[1] Bidgoli, A.M.M., Daneshmehr, A.R., Kolahchi, R., Analytical Bending Solution of Fully Clamped Orthotropic Rectangular Plates Resting on Elastic Foundations by The Finite Integral Transform Method, *Journal of Applied and Computational Mechanics*, 1(2), 2015, 52-58.

[2] Akano, T.T., Fakinlede, O.A., Olayiwola, P.S., Deformation Characteristics of Composite Structures, *Journal of Applied and Computational Mechanics*, 2(3), 2016, 174-191.

[3] Katsikadelis, J.T., Tsiatas G.C., Saint-Venant Torsion of Non-Homogeneous Anisotropic Bars, *Journal of Applied and Computational Mechanics*, 2(1), 2016, 42-53.

[4] Tang, S., Elastic Stresses in Rotating Anisotropic Discs, *International Journal of Mechanical Sciences*, 11, 1969, 509–517.

[5] Murthy, D., Sherbourne, A., Elastic Stresses in Anisotropic Discs of Variable Thickness, *International Journal of Mechanical Sciences*, 12, 1970, 627-640.

[6] Reddy, T.Y., Srinath, H., Elastic Stresses in a Rotating Anisotropic Annular Disc of Variable Thickness and Variable Density, *International Journal of Mechanical Sciences*, 16(2), 1974, 85-89.

[7] Chang, C.I., A Closed-Form Solution for an Orthotropic Rotating Disc, *Journal of Applied Mechanics*, 41(4), 1974, 1122–1123.

[8] Chang, C.I., The Anisotropic Rotating Discs, *International Journal of Mechanical Sciences*, 17(6), 1975, 397-402.

[9] Bert, C.W., Centrifugal Stresses in Arbitrarily Laminated, Rectangular-Anisotropic Circular Discs, *Journal of Strain Analysis for Engineering Design*, 10, 1975, 84-92.

[10] Gurushankar, G.V., Thermal Stresses in a Rotating Nonhomogeneous, Anisotropic Disc of Varying Thickness and Density, *Journal of Strain Analysis for Engineering Design*, 10, 1975, 137-142.

[11] Christensen, R.M., Wu, E.M., Optimal Design of Anisotropic (Fiber-Reinforced) Flywheels, *Journal of Composite*

Materials, 11, 1977, 395-404.
[12] Belingardi, G., Genta, G., Gola, M., A Study of the Stress Distribution in Rotating, Orthotropic Discs, *Composites*, 10(2), 1979, 77-80.
[13] Genta, G., Gola, M., The Stress Distribution in Orthotropic Rotating Discs, *Journal of Applied Mechanics*, 48, 1981, 559-562.
[14] Lekhnitskii, S.G., *Theory of Elasticity of an Anisotropic Body*, Mir Publishers, Moscow, 1981.
[15] Elishakoff, I., Buckling of Polar Orthotropic Circular Plates on Elastic Foundation by Computerized Symbolic Algebra, *Computer Methods in Applied Mechanics and Engineering*, 68(2), 1988, 229-247.
[16] Oilin, H., Oixuan, Z., Ping, W., Guicang, H., A New Method for Calculating Burst Speed of Aeroengine Disks, *ASME-91-GT-121*, 1991, 1-4.
[17] Tutuncu, N., Effect of Anisotropy on Stresses in Rotating Discs, *International Journal of Mechanical Sciences*, 37, 2000, 873–881.
[18] Arnoldi, S.M., Saleeb, A.F., Al-Zoubi, R., Deformation and Life Analysis of Composite Flywheel Disk and Multi-Disk Systems, *NASAffM-2001-210578*, 2001, 1-56.
[19] Zhou, F., Ogawa, A, Elastic Solutions for a Solid Rotating Disc with Cubic Anisotropy, *Journal of Applied Mechanics*, 69, 2002, 81-83.
[20] Callioglu, H., Stress Analysis of an Orthotropic Rotating Disc under Thermal Loading, *Journal of Reinforced Plastics and Composites*, 23(17), 2004, 1857–1869.
[21] Callioglu, H., Thermal Stress Analysis of Curvilinearly Orthotropic Rotating Discs, *Journal of Thermoplastic Composite Materials*, 20, 2007, 357-369.
[22] Callioglu, H., Topcu, M., Altan, G., Stress Analysis of Curvilinearly Orthotropic Rotating Discs under Mechanical and Thermal Loading, *Journal of Reinforced Plastics and Composites*, 24, 2005, 831-838.
[23] Callioglu, H., Topcu, M., Tarakçılar, A.R., Elastic-Plastic Stress Analysis of an Orthotropic Rotating Disc, *International Journal of Mechanical Sciences*, 48, 2006, 985-990.
[24] Sayer, M., Topcu, M., Bektas, N.B., Tarakcilar, A.R., Thermoelastic Stress Analysis in a Thermoplastic Composite Disc, *Science and Engineering of Composite Materials*, 12(4), 2005, 251–260.
[25] Tahani, M., Nosier, A., Zebarjad, S.M., Deformation and Stress Analysis of Circumferentially Fiber-Reinforced Composite Disks, *International Journal of Solids and Structures*, 42(9–10), 2005, 2741–2754.
[26] Koo, K.N., Vibration Analysis and Critical Speeds of Polar Orthotropic Annular Discs in Rotation, *Composite Structures*, 76, 2006, 67-72.
[27] Koo, K.N., Mechanical Vibration and Critical Speeds of Rotating Composite Laminate Discs, *Microsystem Technologies*, 14, 2008, 799-807.
[28] Alexandrova, N., Vila Real, P.M.M., Deformation and Stress Analysis of an Anisotropic Rotating Annular Disk, *International Journal for Computational Methods in Engineering Science and Mechanics*, 9(1), 2008, 43–50.
[29] Nie, G.J., Zhong, Z., Batra, R.C., Material Tailoring for Orthotropic Elastic Rotating Discs, *Composites Science and Technology*, 71, 2011, 406–414.
[30] Durodola, J., Attia, O., Deformation and Stresses in Functionally Graded Rotating Discs, *Composites Science and Technology*, 60, 2000, 987-995.
[31] Chen, J., Ding, H., Chen, W., Three-Dimensional Analytical Solution for a Rotating Disc of Functionally Graded Materials with Transverse Isotropy, *Archive of Applied Mechanics*, 77, 2007, 241-251.
[32] Wang, X., Sudak, L.J., Three-Dimensional Analysis of Multi-Layered Functionally Graded Anisotropic Cylindrical Panel under Thermomechanical Loading, *Mechanics of Materials*, 40(4), 2008, 235–254.
[33] Kansal, G., Parvez, M., Thermal Stress Analysis of Orthotropic Graded Rotating Discs, *International Journal of Modern Engineering Research*, 2(5), 2012, 3881-3885.
[34] Lubarda, V.A., On Pressurized Curvilinearly Orthotropic Circular Disc, Cylinder and Sphere Made of Radially Nonuniform Material, *Journal of Elasticity*, 109, 2012, 103-133.
[35] Peng, X.L., Li, X.F., Elastic Analysis of Rotating Functionally Graded Polar Orthotropic Discs, *International Journal of Mechanical Sciences*, 60, 2012, 84-91.
[36] Boga, C., Analytical and Numerical Axisymmetric Elastic Stress Analyses of Stationary/Rotating Discs Made of Isotropic/Orthotropic Functionally Graded Materials by The Transfer Matrix Method, Ph.D. Thesis, Department of Mechanical Engineering, Çukurova University: No 1698, 2016.
[37] Kacar, I., Yıldırım, V., Effect of the Anisotropy Ratios on the Exact Elastic Behavior of Functionally Power-Graded Polar Orthotropic Rotating Uniform Discs Under Various Boundary Conditions, *Digital Proceeding of ICOCEE – Cappadocia*, Nevsehir, Turkey, 1743-1752, May 8-10, 2017.
[38] Zheng, Y., Bahaloo, H., Mousanezhad, D., Vaziri, A., Nayeb-Hashemi, H., Displacement and Stress Fields in a Functionally Graded Fiber-Reinforced Rotating Disk with Nonuniform Thickness and Variable Angular Velocity, *Journal of Engineering Materials and Technology*, 39, 2017, 031010-1-9.
[39] Aktas, Z., *Numerical Solutions of Two-Point Boundary Value Problems*, Ankara, Turkey, METU, Department of Computer Engineering, 1972.
[40] Roberts, S., Shipman, J., Fundamental Matrix and Two-Point Boundary-Value Problems, *Journal of Optimization Theory and Applications*, 28(1), 1979, 77-88.
[41] Haktanır, V., Kıral, E., Direct Application of Complementary Functions Method to Axisymmetrical Shells and Cylindrical Vaults (Barrels), *Journal of Isparta Engineering Faculty of Akdeniz University*, 6, 1991, 220-239.

[42] Haktanır, V., A New Method for the Element Stiffness Matrix of Arbitrary Planar Bars, *Composite Structures*, 52(4), 1994, 679–691.
[43] Haktanır, V., The Complementary Functions Method for the Element Stiffness Matrix of Arbitrary Spatial Bars of Helicoidal Axes, *International Journal for Numerical Methods in Engineering*, 38(6), 1995, 1031–1056.
[44] Yıldırım, V., Free Vibration Analysis of Non-Cylindrical Coil Springs by Combined Use of the Transfer Matrix and the Complementary Functions Methods, *Communications in Numerical Methods in Engineering*, 13(6), 1997, 487–94.
[45] Kacar, İ., Yıldırım, V., Free Vibration/Buckling Analyses of Non-Cylindrical Initially Compressed Helical Composite Springs, *Mechanics Based Design of Structures and Machines*, 44 (4), 2016, 340-353.
[46] Yıldırım, V., Kacar, I., Introducing a Computer Package Program for Elastic Analysis of Functionally Graded Rotating Thick-Walled Annular Structures, *Digital Proceeding of ICOCEE – CAPPADOCIA*, Nevşehir, Turkey, 1733-1742, May 8-10, 2017.